Coronal Seismology

Laurel Farris
New Mexico State University
laurel07@nmsu.edu

ABSTRACT

Coronal seismology involves the investigation of magnetohydrodynamic (MHD) waves and ocillatory phenomenae that arise in the solar corona. Here some of the dominant waves, oscillations, and modes are intimately investigated in the literature. Analysis of data from the Atmospheric Imaging Assembly (AIA) instrument on the Solar Dynamics Observatory (SDO) is also presented, both as stand-alone research and in the broader context of coronal seismology.

Subject headings: Sun: corona Sun: oscillations Sun: seismology

1. Introduction

The heating of the corona by magnetohydrodynamic (MHD) waves is one of two prevalent theories on how it reaches such high temperatures, the other being magnetic reconnection (Roberts et al. (1984)).

The basic types of MHD waves and oscillations are discussed in §2. §3 discusses each of the research topics in detail, including including references to work that has been done and is currently being carried out to address each one. §5 and §6 include a description of the research project and its implications for the broader field of coronal seismology. Conclusions and future work are summed up in §7.

2. General MHD

2.1. Types of Waves

The categories of MHD waves and oscillations can be best understood by their relative speeds. Figure 1 shows the wave speeds relative to the internal and external Alfvén and sound speeds.

Magneto-acoustic waves can be divided into two categories: slow-mode and fast-mode (Aschwanden (2004)). The slow-mode waves have phase speeds roughly equal to the sound speed in the medium in which they reside, so these are general acoustic, or sound waves.

Fast-mode magnetoacoustic waves have phase speeds close to the Alfvén speed.

2.2. Equations and Models

MHD waves are often modeled with a cylindrical flux tube embedded in a magnetic field.

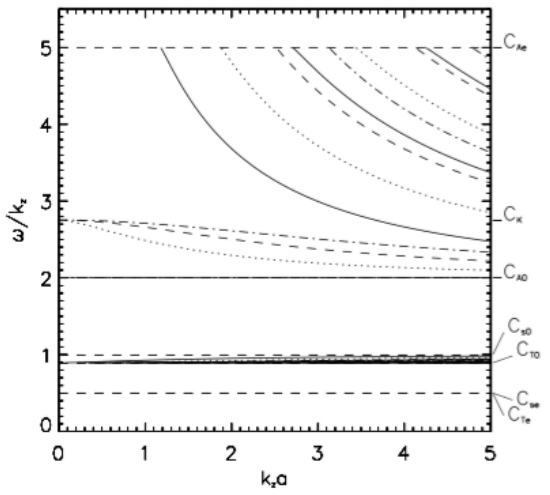

Fig. 1.— text (Image credit: Nakariakov & Verwichte (2005))

[cylindrical model, equations of ideal MHD, etc.]

$$\xi(x) = \xi(r)e^{i(kx+m\phi)} \quad (1)$$

For kink oscillations, m=1, and for sausage modes, m=0.

There are several equations for ideal MHD from which the dispersion relations are derived (I think).

2.3. Excitation and Damping Mechanisms

2.3.1. Resonant Absorption

2.3.2. Phase Mixing

2.4. Observation Techniques

Flux tubes (coronal loops), doppler shift and intensity variations, density variations, velocity and magnetic field values, etc.

3. Research Topics

3.1. Kink Oscillations

Kink oscillations are directly observed in coronal loops in extreme ultraviolet (EUV) wavelengths. They characterize the spacial oscillations that occur over the surface of the loop, perpendicular to the direction traversed by the length of the loop (Nakariakov & Verwichte (2005)). Kink oscillations occur in the "long-wavelength regime"; the product of the wavenumber and the cross-section of the coronal loop is much less than 1 ($ka \ll 1$). The phase speed is just above the Alfvén speed within the loop, and the period of the oscillation is expected to be between $\sim$ 2 and 20 minutes (Aschwanden (2004)).

While temporal variations have been observed previously, spatial variations were not revealed until the launch of TRACE. Some of the first observations of these spatial variations were carried out by Aschwanden et al. (1999), utilizing preliminary data released from the TRACE mission to investigate the oscillations present in coronal loops. Using 171 Å data, they modeled five loops that occompanied a solar flare in 1998. The resulting model had several qualities characteristic of fast kink modes, including asymmetry and displacements represented by sine curves. As the period of kink modes were already known to correlate with the magnetic field strength of the loop, pinpointing this type of mode as the driver in coronal loops provided a valuable constraint on coronal conditions. The absense of any phase shift along the length of the loops revealed that these were *standing waves*, with nodes located at the loop footpoints.

More recently, Pascoe et al. (2015) investigated the driving mechanism behind the production, and damping of kink oscillations. They compared two possible functional form of the damping profile of the driver: that of a Gaussian and an exponential form. While the noise level of the data was too high to distinguish between the two forms, the simulations followed the form of a Gaussian.

They also considered the effect of the spatial profile of the driver itself on the excitation and subsequent damping of the kink waves. Two different possiblilities were explored here: the effect of a "highly structured" driver, which they found to be unrealistic, and the effects of eddies and photospheric motions around the footpoints of the coronal loops.

3.2. Sausage Oscillations

Lopin & Nagorny (2015) plotted the changes in intensity and cross-sectional area for sausage oscillations in photospheric pores extending up through the solar atmosphere. They used the general cylinder model for the pores, though it is more likely that the cross-sectional area of the waveguide increases with height as the temperature increases and density drops. The relationship between pore size and intensity can indicate

3.3. Acoustic Oscillations

The relatives periodicities of aacoustic oscillations were recognized as important characteristics, and modelled by Roberts et al. (1984). They recognized magnetoacoustic oscillations as a useful way to determine other properties of the solar atmosphere.

Srivastava & Dwivedi (2010) used intensity oscillations of a few different ionization species to pinpoint the orgin and progression of magnetoacoustic waves between bright points in the photosphere, through the transition regions, and up into the corona. The time series of intensity oscillations was converted into a power spectrum, and periodicities were extracted using wavelet analysis and periodograms (note here on what exactly these are?). The periods they derived ($\sim 263 \pm 80$ s for the He II 256.32 Å emission line and ($\sim 241 \pm 60$ s for the Fe XII 195.12 Å emission line) were close to the 5-minute global oscillations of the sun.

3.4. Propagating Acoustic Waves

While standing acoustic waves are primarily seen in closed coronal loops, propagating waves

have been observed in both closed and open structures. The propagation speed of such waves is much lower than the local Alfvén speed, thus they are categorized as slow, longitudinal waves, (or magnetoacoustic waves), that travel along magnetic field lines at speeds roughly equal to the local sound speed. The changes in intensity along the same location as these waves propagate in time are mapped side by side to give time-distance information. The period, wavelength, propagation speed, and amplitude can all be derived using this method. Since the local sound, c_s is related to temperature, T, as

$$c_s \propto \sqrt{T} \tag{2}$$

a difference in observed propagation speeds implies a changing temperature profile in the transverse direction across the loop. (Nakariakov & Verwichte (2005)).

One of the first studies to analyze simultaneous observations at different wavelengths was carried out by Robbrecht et al. (2001) using data from two different instruments: the Extreme ultraviolet Imaging Telescope (EIS) on the Solar and Heliospheric Observatory (SOHO) and the Transition Region And Coronal Explorer (TRACE). These wavelengths, along with their corresponding ions emitting at those wavelengths, the temperature, and other relevant quantities from the study are given in table 1. Both instruments observed AR

instrument	EIT	TRACE
ion	Fe XII	Fe IX
wavelength	195 Å	171 Å
cadence	15 s	25 s
temperature	1.6 MK	1 MK
sound speed	192 km s^{-1}	152 km s^{-1}
propagation speed	110 km s^{-1}	95 km s^{-1}

Table 1: Relevant quantities from Robbrecht et al. (2001)

8218, where the presence of "weak transient disturbances" were revealed, and later classified as slow, propagating magnetoacoustic waves, with speeds that varied between 65 and 150 km s^{-1}. The expression for the formal sound speed of the ambient region was given by

$$c_s = 152\ T^{1/2}\ \text{m s}^{-1} \tag{3}$$

where T is in units of Kelvin. This was compared to the observed speed of the progating wave, which was derived from the slope of the "ridges" on each of the four time-distance plots. The propatation speed of each wave was slightly ($\sim$ same order of magnitude) lower than the local sound speed. This difference was due to the angle between the loop and the plane of the sky against which the observations were made. The amount of time for a disturbance to pass a particular point was determined to be $\sim$ 169 s from the TRACE data. As both observations targeted the same wave, the signficance of the differing speeds for each observation indicated a temperature gradient in the loop itself, indicating either a bundle of loop threads that make up a single loop, or a number of concentric shells that make up a single loop.

A similar analysis in multiple wavelengths was carried out by Uritsky et al. (2013), using about 6 hours of observational data from the Atmospheric Imaging Assemply (AIA) on the Solar Dynamics Observatory (SDO). In addition to these observations, they introduced the "surfacing transform technique" in order to address the difficulty in extracting information from these low-amplitude waves amidst the noise (a typical signal-to-noise (S/N) ratio was $\sim$ 0.1 %). (more information about this technique here?) This method involved the resonant behavior of "surfing signals", revealed during quasi-periodic disturbances.

This technique was applied to the lines at 131 Å, 171 Å, 193 Å, and 211 Å, over the active region (AR) NOAA AR 11082, where no sunspots were seen to be present and the flares were relatively low-energy. They found the same relationship between sound speed and temperature as shown in equation 2, though the driving mechanism for these disturbances was uncertain. The observed propagations were travelling primarily in the upward direction away from the footpoint, at speeds of about 40 to 180 km s^{-1} and periodicities between 4 and 8 minutes over all four channels.

Type of wave	Timescales	Sizescales	Observational techniques
Kink Oscillations	short	short	something
Sausage Oscillations	short	short	something
Acoustic Oscillations	x	x	x
Propagating	x	x	x

3.5. Propagating Fast Waves

3.6. Torsional Modes

3.7. Mixed Modes

4. Discussion

The observational techniques and relevant properties of each of the different kinds of MHD waves are summarized in table 1.

5. Data

As part of the general topic of coronal seismology, a small research project was carried out as well, continuing over from several semesters previously. Several of the observational and analytical methods used in the literature were reproduced for this project.

6. Analysis

7. Conclusion

And we're finished.

REFERENCES

Aschwanden, M. 2004, Springer

Aschwanden, M. J., Fletcher, L., Schrijver, C. J., & Alexander, D. 1999, The Astrophysical Journal, 520, 880

Lopin, I., & Nagorny, I. 2015, ApJ, 810, 87

Nakariakov, V. M., & Verwichte, E. 2005, Living Rev. Solar Phys.

Pascoe, D. J., Wright, A. N., De Moortel, I., & Hood, A. W. 2015, A&A, 578, A99

Robbrecht, E., Verwichte, E., Berghmans, D., et al. 2001, A&A, 370, 591

Roberts, B., Edwin, P. M., & Benz, A. O. 1984, ApJ, 279, 857

Srivastava, A. K., & Dwivedi, B. N. 2010, MNRAS, 405, 2317

Uritsky, V. M., Davila, J. M., Viall, N. M., & Ofman, L. 2013, ApJ, 778, 26

This 2-column preprint was prepared with the AAS LaTeX macros v5.2.